THE JOURNAL OF PHYSICAL CHEMISTRY C

Article

pubs.acs.org/JPCC

Controlling Adsorption Structure of Eosin Y Dye on Nanocrystalline TiO_2 Films for Improved Photovoltaic Performances

Fan Zhang, Feng Shi, Wei Ma, Fei Gao, Yang Jiao, Hui Li, Jingchuan Wang, Xinyan Shan, Xinghua Lu, and Sheng Meng*

Beijing National Laboratory for Condensed Matter Physics, and Institute of Physics, Chinese Academy of Sciences, Beijing, 100190, P. R. China

ABSTRACT: Adsorption structure of Eosin Y dyes on nanocrystalline TiO_2 can be manipulated by adding a small fraction of water into organic electrolyte. Binding mode switching from hydrogen bonded monodentate to bidentate bridging configuration has been observed and confirmed by Raman and infrared spectroscopy measurements, with vibration peaks assigned using density functional theory calculations. Photovoltaic measurements on the fabricated dye-sensitized solar cells indicate that energy conversion efficiency is enhanced by manipulating molecular adsorption configuration of Eosin Y dyes. This opens a new avenue to improving photovoltaic performance by suppressing unfavorable adsorption configurations in dye solar cell devices.

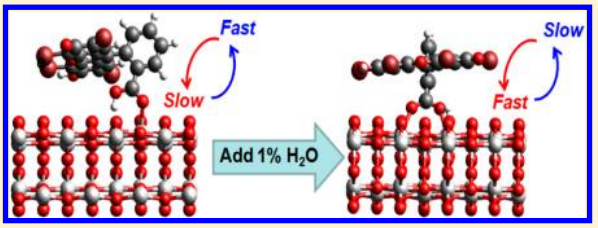

INTRODUCTION

The dye-sensitized solar cell (DSC), invented by Prof. M. Grätzel at École Polytechnique Fédérale de Lausanne in 1991,[1] is a promising route toward low-cost, environment friendly power generation, which uses dye molecules adsorbed on the nanocrystalline oxide semiconductors such as TiO_2 to collect sunlight. In a DSC, light absorption (by dyes) and charge collection (by semiconductors) processes are separated, mimicking natural light harvest in photosynthesis. Only when dye molecules effectively bind to TiO_2 surface can the following processes such as charge injection and transportation proceed with high efficiency. For the majority of dyes, a carboxyl group is employed as an effective anchor through which dyes bind onto TiO_2 surfaces. It is well-known that the adsorption geometry has a remarkable influence on photovoltaic parameters of DSC such as the open circuit voltage and short circuit current. De Angelis et al. investigated the adsorption configuration of most popular Ru-complex N-719 dye on TiO_2 and showed that the dipole moment orientation of the sensitizers resulted from different binding configurations, which can lead to as large as a 0.61 eV shift in TiO_2 conduction band edge (CBE), introducing a larger open circuit voltage (V_{oc}).[2] Jiao et al. studied all organic cyanoacrylic dyes and concluded that the adsorption configuration with Ti−N binding is beneficial to electron injection, which improves short circuit current.[3]

However, the precise interface structures upon dye adsorption on TiO_2 have been under heavy debate for decades with controversial conclusions. Taking N-719 dye as an example, three adsorption configurations were proposed: monodentate, bidentate chelating, and bidentate bridging modes.[4] To find out which one dominates in real systems, Grätzel et al. investigated Ru complex dyes by Fourier transform infrared (FTIR) spectroscopy according to the Deacon-Philips rule.[5] This rule introduces an important parameter $\Delta\nu$, which is the frequency splitting of surface bound carboxylate stretching bands, asymmetric and symmetric vibrations, measured by infrared (IR) or Raman spectroscopy. Two cases are compared: $\Delta\nu$ for dyes in solid state, $\Delta\nu$(solid), and $\Delta\nu$ for adsorbed dyes, $\Delta\nu$(ads). If $\Delta\nu$(ads) > $\Delta\nu$(solid), the dye molecule takes a monodentate binding mode; if $\Delta\nu$(ads) < $\Delta\nu$(solid), the bidentate bridging mode is more preferred; if $\Delta\nu$(ads) ≪ $\Delta\nu$(solid), the chelating mode is most likely to present. For N-719, $\Delta\nu$ (ads) = 227 cm^{-1} and $\Delta\nu$ (solid) = 243 cm^{-1}, thereby Grätzel et al. proposed that N-719 dye adsorbs on TiO_2 in a bidentate bridging mode.[6] Lee et al. went further and suggested that hydrogen bonds also participate in dye adsorption.[7] Nevertheless, the Deacon-Philips rule is empirical, which cannot designate dye adsorption mode precisely. In practice, it is also challenging to distinguish the symmetric vibration of the COO group (located at ca. 1300−1500 cm^{-1}) from other vibration modes in IR or Raman spectra of a complex molecule, because the bending and wagging vibration modes of CH_2 or CH_3 are also located in the same frequency region. It should be noticed that all previous studies mentioned above only dealt with solid state samples, which were different from the practical systems containing liquid electrolytes. Therefore, identifying the adsorption structure of dyes in a realistic device environment in the presence of liquid electrolyte is more important for DSC developments and of course much more challenging.

With many advantages over Ru complex dyes, metal-free organic dyes have attracted much attention in DSC field recently. Eosin Y (EY), a popular organic pigment with

Received: May 5, 2013
Revised: June 21, 2013
Published: June 21, 2013

   dx.doi.org/10.1021/jp404439p | J. Phys. Chem. C 2013, 117, 14659−14666

excellent light harvesting property, with low cost, and often used as a fluorescent dye in biological research, has been used in DSC[8,9] and reached an efficiency[10] of 2.0%. As a xanthene dye with only one carboxyl group, it is also a simple model for investigating dye binding configurations of carboxylic dyes on the TiO_2 surface. In the present work, we have taken the EY molecule as a representative dye to study dye adsorption on TiO_2 by combining vibration spectroscopic measurements and first-principles calculations. We first measure the photoabsorption spectrum of EY dye to identify its molecular forms before attaching to TiO_2. Dye adsorption introduces optical band broadening and frequency shift. Two different binding configurations, hydrogen bonded monodentate and bidentate bridging, were clearly identified by comparing spectroscopic FTIR and Raman measurements with theoretical analysis. More importantly, the proportion of the bidentate dye adsorption mode can be adjusted by the presence of a small amount of water in the organic electrolyte, which has an important influence on DSC's photovoltaic performance.

EXPERIMENTAL SECTION

Materials and Chemicals. EY (99%, powder) from Sigma Aldrich, N-719 (99%) from Solaronix, P25 TiO_2 nanoparticles (99.5%), and 200 nm particle from Degussa are all commercially available and used as received without further purification. Confirmed by Raman and X-ray diffraction, anatase content is over 90% in our P25 TiO_2 sample. Other regents such as ethanol or acetonitrile are analytically pure.

Absorption, Raman, and IR Spectra. A layer of nanocrystalline TiO_2 (5 μm) was deposited on a precleaned glass substrate by doctor blade method using a uniform TiO_2 paste containing 3.5 g Degussa P25 TiO_2 powder and 35 mL ethanol. TiO_2 film was heated to 500 °C in the muffle furnace and kept at that temperature for 30 min to remove organic pollutants. When it was cooled to 100 °C, it was immersed into 0.4 mM EY ethanol solution immediately and maintained for 15 h, and then the film was rinsed with pure ethanol thoroughly to remove unbound dye molecules and dried in air. Absorption spectra were recorded by spectrophotometer, model iHR320, Horiba.

To measure Raman spectra, the sensitized TiO_2 powder was removed from the glass and contained in nuclear magnetic resonance (NMR) tubes and sealed. A NICOLET 6700 FT-Raman spectrometer (Thermo Scientific, USA) was applied. The wavelength used was 1064 nm to avoid fluorescence effect and a frequency resolution of 4 cm^{-1} was achieved.

Infrared spectra were obtained using a NICOLET iN10 MX FTIR spectrometer (Thermo Scientific, USA). A small volume powder of EY and dye adsorbed TiO_2 was pressed between two diamond windows. Spectra covering the range from 4000 to 600 cm^{-1} and 16 scans at a resolution of 4 cm^{-1} were used. The IR illuminating area was about 100 μm × 100 μm.

DSC Fabrication. The procedure for DSC fabrication and assembly followed the description in ref 11. Fluorine-doped tin oxide coated glass (FTO, NSG) was cleaned by sequential sonication in distilled water, acetone, and ethanol and then treated in UV-ozone furnace for 20 min. A compact TiO_2 blocking layer was deposited on the conductive side of FTO glass by soaking the substrate in 40 mM $TiCl_4$ aqueous solution and heated to 70 °C for 30 min. After rinsing with distilled water and dried in air, a layer of nanocrystalline TiO_2, 10 μm thick, was deposited by doctor blade method, using a uniform TiO_2 paste containing 3.5 g Degussa P25 TiO_2 powder and 0.17 g carbowax M-20,000 in 35 mL ethanol. Following that, a layer of light-scattering TiO_2 containing 200 nm particles, 4 μm thick, was deposited on P25 TiO_2 film, then dried in air for 5 min, and heated to 450 °C for 30 min. After cooling to room temperature, the film was soaked in 40 mM $TiCl_4$ solution again and boiled at 70 °C for 40 min. After washing it with distilled water, we heated the TiO_2 film gradually to 500 °C (8 °C/min), maintained it at 500 °C for 30 min, and then cooled it to 100 °C. We then immersed the film into N-719 or EY ethanol solution (0.4 mM) and sensitized them overnight. After 15 h, we took the film out of dye solution and rinse it with ethanol. It was dried in a 60 °C oven. Plastic spacers were prepared and put on the dye adsorbed TiO_2 film. The electrolyte was dropped onto the film. For the EY based cell, the electrolyte was NaI 0.5 M, I_2 0.05 M in pure actonitrile or in acetonitrile containing 1% or 2% water. For the N-719 cell, a standard electrolyte was used. The standard electrolyte contains DMPII 0.3 M, I_2 0.05 M,LiI 0.5 M, 4-TBP 0.5 M in acetonitrile. Finally, the anode and Pt counter electrode were fixed together to make the DSC device.

Current density−voltage ($I-V$) curves of DSCs with 0.16 cm^2 active area were obtained under AM 1.5G (100 mW/cm^2) illumination. The measurement employed a solar simulator equipped with 150W xenon lamp (model no. 94021A, Oriel), a reference solar cell (model no. 91150 V), and a Keithley model 2400 digital source meter.

Theoretical Computation. First-principles density functional theory (DFT)[12] calculations were carried out to study the molecular geometry, electronic structure, vibration spectrum and the UV−vis spectra of EY adsorbed onto TiO_2 surfaces. The ground-state molecular geometries were optimized with VASP, using Vanderbilt ultrasoft pesudopotentials and generalized gradient approximation (GGA) of PW91.[13,14] An energy cutoff of 400 eV and Γ point k-sampling was used. Geometries were optimized until forces on nonfixed atoms are below 0.04 eV/Å, which were considered fully relaxed. The simulation cell contains the EY chromophores, bonded onto the TiO_2 anatase (101) surface, the dominant and thermodynamically stable facet.[15] The surface slab has dimensions of 20.77 × 15.27 × 20.00 $Å^3$, corresponding to a TiO_2 surface coverage of one dye per 317 $Å^2$ or 0.5 $\mu mol \cdot m^{-2}$. Periodic boundary conditions were applied to replicate the simulation cell in all three dimensions. A sufficient large vacuum layer (at least 10 Å) was added to the simulation cell in the direction perpendicular to the surface to ensure that no interactions between each slab. Vibration frequency was calculated from diagonalizing the force constant matrix to produce eigen values of the matrix, which correspond to the energy of normal vibration modes. The maximum change in the interface bond length is 0.02 Å in order to retain the validity of harmonic approximation. Optical absorption spectra were calculated based on linear response time-dependent DFT (TDDFT) using the Perdew−Burke−Ernzerhof (PBE) functional and 6-31G(d) basis set, as implemented in Gaussian 09 program. The polarizable continuum model (PCM)[16] was used to account for the solvation effect (in ethanol).

RESULTS AND DISSCUSION

Photoabsorption Spectrum. Eosin Y is subject to a tautomeric equilibration between many structures (lactone, quinonoid and their derivatives), affected by pH and other conditions of the solution.[17] The molecular structure of EY in the quinonoid form is shown in Figure 1a. Since EY is an acid,

dx.doi.org/10.1021/jp404439p | J. Phys. Chem. C 2013, 117, 14659−14666

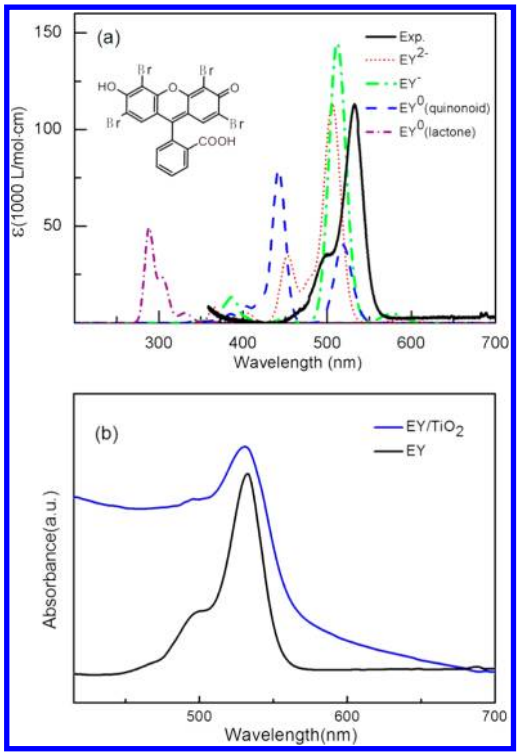

Figure 1. (a) Experiment photoabsorption spectrum of EY dissolved in ethanol solution with concentration of 1×10^{-5} M. Also shown are calculated absorption spectra of different possible EY molecular structures. The inset shows the EY molecule in the neutral quinonoid form. (b) Photoabsorption spectrum of EY adsorbed on the TiO_2 film with a thickness of 5 μm (blue curve), compared with that for EY in ethanol (black curve).

the hydrogen atom of the hydroxyl group on the xanthene moiety and that on the carboxylic group may dissociate in solutions, forming a monoanion or dianion. Judging from the Henderson−Hasselbalch equation, which employs the pH value, and the pK_a constant for proton dissociation, as a measure of acidity, the hydroxyl on xanthene group (pK_a = 7.7) can release proton much more easily than the carboxylic group (pK_a = 9.8) in ethanol.[17] Therefore, monoanion EY^- corresponds to a structure with the deprotonated hydroxyl group, and dianion EY^{2-} has both protons missing. The lactone form of EY is a cyclic ester with two hydroxyls sitting on each side of the xanthene ring and COO binding to the center carbon of xanthene group, which can be seen as the condensation product of the carboxylic group in the same molecule.

To find out the exact molecular structure of EY before binding to TiO_2, we measured the absorption spectrum of EY in ethanol, as shown in Figure 1. The photoabsorption curve displays a distinct peak at 532 nm and a small shoulder at 496 nm. Measured molar extinction coefficient at 532 nm is 1.10×10^5 M^{-1} cm^{-1}, which is in good agreement with the reported value[18] of 1.12×10^5 M^{-1} cm^{-1}. The shape of the absorption curve and peak location are similar to absorption spectrum of dianion EY^{2-} in water solutions,[19] implying the existence of the dianion form of EY in ethanol.

To make a more precise assignment, we calculated photoabsorption spectra for all possible molecular structures based on TDDFT, all shown in Figure 1a. Absorption maximum of dianion, monoanion, neutral quinonoid and neutral lactone forms of EY locates at the wavelengths of 506, 512, 443, and 288 nm, respectively. Compared to experimental absorption spectrum, the calculated spectra for dianion and monoanion are closest to the measured one. The neutral quinonoid and lactone form cannot be dominant due to their obvious discrepancy with experimental spectroscopy. In addition, the shoulder at ∼460 nm for dianion absorption also agrees with the appearance of the shoulder in experiment. Very likely, EY in ethanol solution is a mixture with dianion and monoanion as dominant species.

Figure 1b shows the photoabsorption spectra of EY adsorbed on TiO_2. For a direct comparison, the spectrum of free EY ethanol solution in Figure 1a is also shown. We found that the absorption peak is only slightly blue-shifted from 532 to 530 nm when EY binds onto TiO_2; more importantly, the main absorption peak is much broadened with a long tail extending into the red-yellow region at ∼550 nm. A small shoulder could still be discernible at 496 nm upon EY adsorption; however, its strength relative to the main absorption peak is much more attenuated compared to free EY solution. The larger absorption background at the short wavelength end is due to intensive absorption of TiO_2 substrate and its defects.

Comparing the photoabsorption spectrum before and after EY adsorption onto the TiO_2 surface, one can infer that EY molecules mainly keep their original forms as in ethanol, namely, in the mixed dianion and monoanion forms. However, both the attenuation of the 496 nm shoulder and the tail at the red end imply that lots of EY molecules turn from the dianion to the monoanion configuration after surface adsorption, since EY^- has more intense absorption in longer wavelengths compared to EY^{2-} dianions. This observation is consistent with the fact that the TiO_2 surface is more acidic than the bulk ethanol solution (the pH value at TiO_2 surface[20] is below 6.2, the isoelectric point of P25 TiO_2). Consequently, EY^{2-} receives protons from the acidic environment in the vicinity of the TiO_2 substrate and become more protonated. Neutral quinonoid and lactone configurations may also exist when bound to TiO_2, but they cannot be dominant species judging from the shape of photoabsorption spectrum in Figure 1b. Therefore in the following discussion we mainly focus on the anion forms of EY for simplicity, and when needed we also take the lactone isomer for comparison.

Raman and IR Spectra of Eosin Y Adsorbed on TiO_2. Direct evidence concerning EY adsorption configuration on TiO_2 surface can be obtained by measuring the vibrational spectra of EY molecules at the interface. Figure 2a,c presents the IR and Raman spectrum of EY molecules in the powder form. The band at 1753 cm^{-1}, observed both in IR and Raman, is assigned to C═O stretching of a free carboxyl group. It completely disappears after EY adsorption on TiO_2 (Figure 2b,d), strongly suggesting that EY molecules adsorb on TiO_2 via its carboxyl group. In the IR spectrum of EY adsorbed TiO_2 film (Figure 2b), a broad band appears at 1640 cm^{-1}, which is assigned to the scissoring mode of liquid water.[21] This assignment is consolidated with the IR spectrum of bare TiO_2 surface without EY adsorption but may inevitably bound with water molecules (dotted line, Figure 2b). This band may interfere with the asymmetric COO stretch mode, ν_{asym}(COO), of the carboxylic group. Whereas in the Raman spectrum (Figure 2d), water scissoring vibration is very weak due to its Raman-insensitivity, it cannot influence the assignment of intense peaks in this frequency region. Based on above considerations, we mainly focus on the Raman spectrum analysis.

dx.doi.org/10.1021/jp404439p | J. Phys. Chem. C 2013, 117, 14659−14666

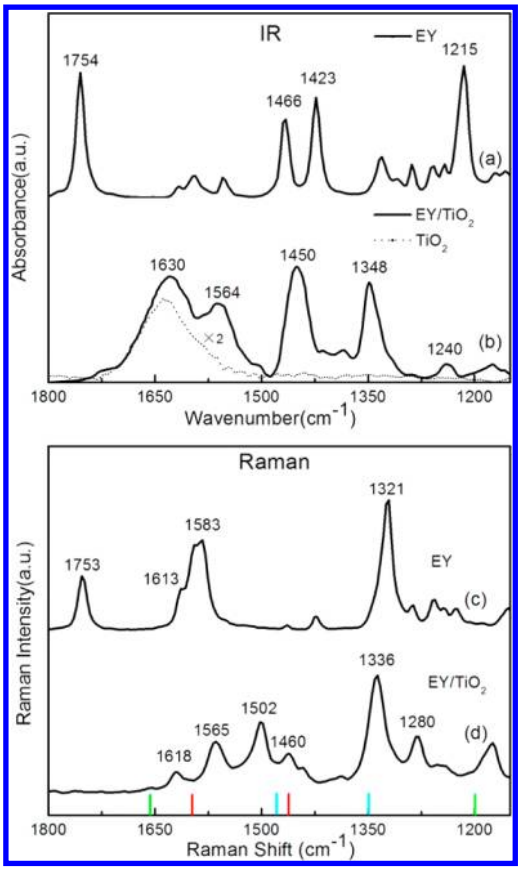

Figure 2. IR spectrum of (a) EY powder and (b) EY adsorbed TiO_2. Raman spectrum of (c) EY powder and (d) EY adsorbed TiO_2. Theoretical frequencies of EY/TiO_2 are shown as vertical bars in (d). Red bars for configuration I: $\nu_{asym}(COO)$ = 1597 cm^{-1}, $\nu_{sym}(COO)$ = 1460 cm^{-1}; blue for configuration II: $\nu_{asym}(COO)$ = 1480 cm^{-1}, $\nu_{sym}(COO)$ = 1349 cm^{-1}; green for configuration III: $\nu_{asym}(COO)$ = 1656 cm^{-1}, $\nu_{sym}(COO)$ = 1197 cm^{-1}.

In Raman spectra, a distinct peak at 1618 cm^{-1} of the adsorbed dye arouses our interest (Figure 2d). Assignment of the peaks around 1600 cm^{-1} in vibrational spectra for dye adsorbed TiO_2 has been debated for years, particularly on whether it is the vibration mode of a phenyl group, or a xanthene group,[22] or the asymmetric vibration mode of a COO group.[23] To ascribe the peaks more precisely, we have calculated the binding energy and vibration frequency of COO group from all possible EY adsorption structures, as displayed in Figure 3. Adsorption configuration I is the monodentate adsorption mode with an additional hydrogen bond connected to the O atom of the TiO_2 substrate, referred to as H-bonded monodentate, or HM adsorption mode here. Model configuration II is the bidentate bridging mode with two interface Ti−O bonds, abbreviated as BB mode. For comparison we also consider configuration III, where EY dye adsorbed in the intact lactone form via a single Ti−O bonding to TiO_2 surface, referred to as M adsorption configuration. The dye adsorption energy (E_{ads}) for configration I (HM) and II (BB) is 0.69 and 0.61 eV, respectively. The energy difference is within the accurary of DFT simulations, especially considering that above energies do not take into account the solution eviroment such as pH values. From calculated adsorption energy, both structures can exist. The relative adsorption energy for configuration III (M mode) is small, 0.36 eV, due to the high stability of the lactone form of EY in free space.

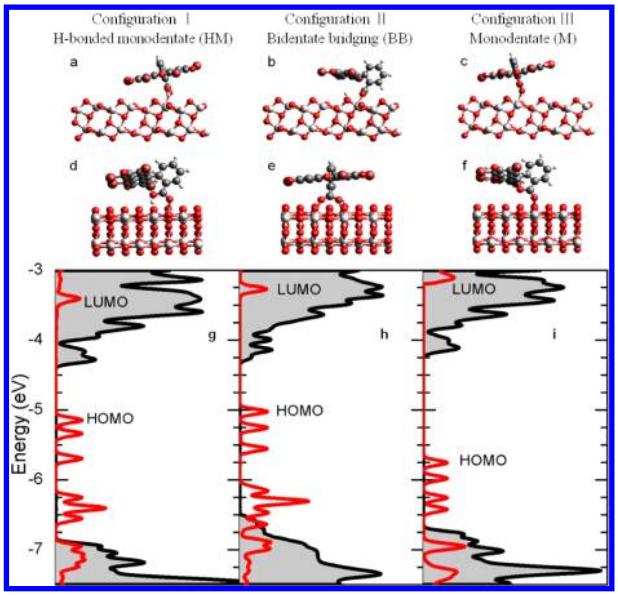

Figure 3. (a−c) Front view and (d−f) side view of EY adsorption configurations I−III. (g−i) Calculated projected density of states for configurations I−III. Red curves are for EY dyes, and shaded areas under black lines are for TiO_2 substrate.

Adsorption of EY in lactone form is thus less plausible, which could easily desorb from the TiO_2 substrate. To judge which structure exists in the real system, Raman shift related to the carboxyl group in these configurations provides a clue.

The location of the calculated peaks for COO asymmetric and symmetric vibration modes is represented by short vertical bars in Figure 2d. Theoretical results show that the frequency of asymmetric COO vibration in the HM configuration, $\nu_{asym}(COO)$ = 1597 cm^{-1}, is the most close to the value of 1618 cm^{-1} measured in Raman experiment. Therefore, the 1618 cm^{-1} peak may indicate the existence of HM adsorption mode for EY/TiO_2. The symmetric mode of COO in HM configuration is calculated to be $\nu_{sym}(COO)$ = 1460 cm^{-1}. We note that both the asymmetric and symmetric COO vibration modes in a neutral carboxyl acid group are Raman active. Above 1618 cm^{-1}, no obvious band is observed, indicating little molecules adsorb on TiO_2 with structure M, whose $\nu_{asym}(COO)$ = 1656 cm^{-1}. As for BB adsorption structure, it is hard to confirm its appearance in Figure 2d alone, because $\nu_{asym}(COO)$ in this configuration (1480 cm^{-1}) is not Raman active. In IR spectrum this mode is buried up by phenyl vibration bands at 1450 cm^{-1}. Fortunately, a peak located at 1348 cm^{-1} shows up after EY adsorption in the IR spectrum (Figure 2b), which matches very well the calculated value for symmetric COO vibration, $\nu_{sym}(COO)$ = 1349 cm^{-1}, for configuration BB. Combined with both Raman and IR spectra, there is a great possibility that BB configuration also exists during EY adsorption.

Our assignments are in good agreement with previous investigations. For example, peaks in Figure 2d are very similar to surface enhanced Raman signal of chemisorbed EY on alumina/Ag substrate.[24] Formic acid and ascorbic acid adsorption on TiO_2 were studied using Raman spectroscopy by Gomez et al.,[25] in which the peaks at 1610 cm^{-1} and 1619 cm^{-1} were observed and attributed to the $\nu_{asym}(COO)$ mode in HM configuration. Amino acid adsorption on TiO_2 was also studied by Guczi et al. with sum frequency generation vibrational spectroscopy. The peak at 1627 cm^{-1}, which is

dx.doi.org/10.1021/jp404439p | J. Phys. Chem. C 2013, 117, 14659−14666

Raman active, was assigned to a strongly hydrogen bonded asymmetric carboxylate stretch.[26] Therefore, we conclude that, to discern the adsorption structure of chemicals with a carboxyl group, bands located between 1600 cm^{-1} to 1630 cm^{-1} may be a sensitive sign for the hydrogen bonded monodentate adsorption mode. More evidence to support the above assignments come from additional experiments by adjusting electrolyte discussed below.

Structural Changes in Solution. In real DSC devices, the dye/TiO_2 nanoparticles are immersed in electrolyte solutions that may lead to a different Raman behavior. This could possibly be utilized to assist assigning Raman peaks in Figure 2d. Figure 4 displays the Raman spectra of EY/TiO_2 measured

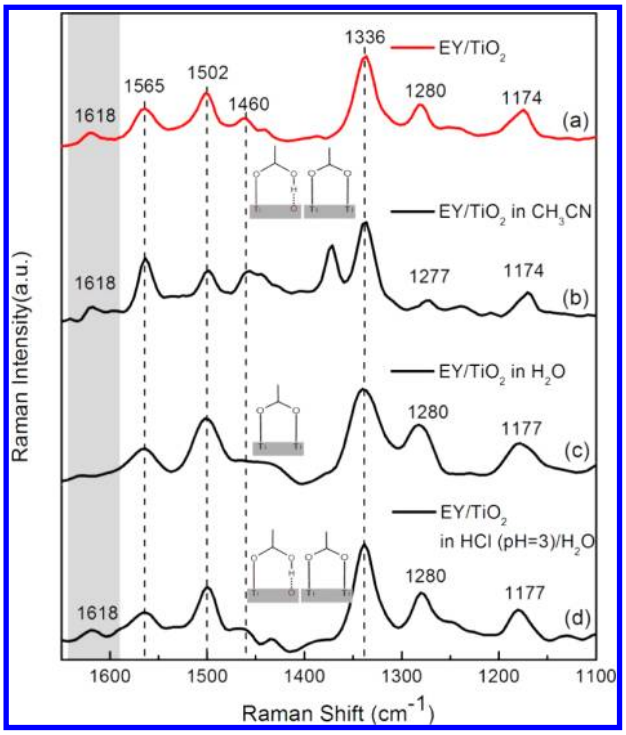

Figure 4. Raman spectrum of EY adsorbed TiO_2 under different conditions: (a) in air, (b) in acetonitrile, (c) in pure water, and (d) in HCl aqueous solution at pH 3.

under different electrolyte conditions. It is clearly shown that the Raman spectrum for EY/TiO_2 in acetonitrile (Figure 4b) is a combination of features for the bare EY/TiO_2 nanoparticles (Figure 2d) and pure acetonitrile solvents (a peak at 1373 cm^{-1} and a broad band at 1445 cm^{-1}). It suggests that there is no obvious structural change upon immersing the EY/TiO_2 nanoparticles in acetonitrile. However, the Raman spectra are quite different in aqueous environment (Figure 4c). The peak at 1618 cm^{-1} disappears completely in water and that located at 1460 cm^{-1} seems to fade away too, while other bands are largely unchanged. This implies the behavior of the two peaks at 1618 and 1460 cm^{-1} are different from those at 1565, 1502, and 1336 cm^{-1}. The latter bands are assigned to vibration modes of the xanthene or phenyl groups.[23] Since the location of the former two peaks are close to the calculated COO vibration frequency in H-bonded monodentate adsorption, it is reasonable to ascribe them to the ν_{asym}(COO) and ν_{sym}(COO) in the HM configuration, as discussed in previous section. The disappearance of 1618 and 1460 cm^{-1} peaks in water strongly suggests EY adsorption mode switches from configuration HM to configuration BB. Accordingly, features at 1348 cm^{-1} are also strengthened. Adsorption structure switch induced by water can be explained by the pK_a value of the carboxyl group in EY. In aqueous environment, the pK_a of EY carboxyl[27] is 3.75, which is much below the pH value of P25 TiO_2-water system (~6.2).[28] According to the Henderson–Hasselbalch equation, when EY-bonded TiO_2 surface is immersed in water, the hydrogen atom of carboxyl group dissociates and transfers to the solution or to TiO_2 surface, leading to an adsorption structure transition from configuration HM to configuration BB.

To further confirm our analysis, we added HCl aqueous solution (pH 3) into EY adsorbed TiO_2 powder. As expected, the 1618 cm^{-1} peak reappeared (Figure 4d), and the band at 1460 cm^{-1} is recovered simultaneously, indicating that the HM adsorption is restored at low pH. In the presence of HCl solution, the protonation process of EY carboxyl group takes place since the pH value is lower than its pK_a value. This presents additional strong evidence to further support the assignment of 1618 and 1460 cm^{-1} peaks to ν_{asym}(COO) and ν_{sym}(COO) in the HM adsorption mode.

Influence of Adsorption Structure on DSC Performance. Manipulating dye adsorption structures provides a simple effective way to improve DSC performances. Inspired by above observation that EY dye adsorption can switch from H-bonded monodentate in acetonitrile to bidentate bridging configuration in water, we take this wisdom to adjust the binding mode of EY on TiO_2 to see whether the photovoltaic performance of DSC device can be improved. Figure 5 shows

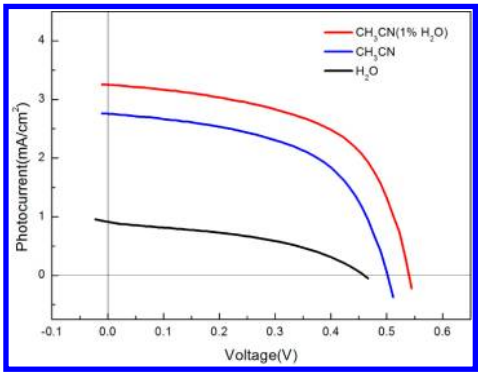

Figure 5. Current–voltage (I–V) curves for dye solar cells applying pure water, pure acetonitrile, or acetonitrile with 1% water as liquid electrolyte, measured under AM 1.5G (100 mW/cm^2) illumination.

the measured I–V characteristics of DSC fabricated with EY in different electrolytes. Key parameters of the DSC devices including short-circuit photocurrent J_{sc}, open-circuit voltage V_{oc}, and fill factors (FF) are listed in Table 1, together with the overall sunlight-to-electricity conversion efficiency (η). As a

Table 1. Performance Characteristics of EY-Based Dye Solar Cells Applying Different Electrolytes

cell	dye	electrolyte	V_{oc} (V)	J_{sc} (mA/cm^2)	FF	η (%)
#1	EY	acetonitrile	0.50	2.7	0.55	0.75
#2	EY	acetonitrile (1% water)	0.54	3.2	0.57	0.98
#3	EY	acetonitrile (2% water)	0.53	3.2	0.56	0.95
#4	EY	water	0.46	0.91	0.43	0.18
#5	N-719	acetonitrile	0.73	13.5	0.66	6.5

dx.doi.org/10.1021/jp404439p | J. Phys. Chem. C 2013, 117, 14659–14666

reference, the DSC device with N-719 as the sensitizer reaches a high efficiency η = 6.5%, indicating the quality of TiO_2 film and counter electrode is reliable. For EY based devices, four kinds of electrolyte containing 0.5 M NaI and 0.05 M I_2 are applied. The solvent for electrolyte #1 is purely acetonitrile, and the device reaches an efficiency of η = 0.75%. Electrolyte #2 differs from electrolyte #1 by adding extra 1% (volume) water. As a result, open circuit voltage V_{oc} of cells with electrolyte #2 is improved from 0.50 to 0.54 V and the efficiency is increased by ~30% (see Table 1). When water amount in acetonitrile is increased to 2% (electrolyte #3), no further photovoltaic improvement is obtained compared to cells with electrolyte #2, indicating that 1% water in acetonitrile is the optimized level. After further optimizing film thickness and related parameters, the efficiency of devices with electrolyte #1 and #2 can reach efficiency values of η = 1.5% and 1.8%, respectively. The trend in V_{oc} remains the same, namely, an increase by about 40 meV is persistent with 1% water adding to the electrolyte. Since the amount of water added in electrolyte is tiny, we believe it cannot impose a significant influence on the transport property of TiO_2 and that of ions in electrolyte.

The mechanism mentioned above gives us invaluable insight into the relationship between the adsorption structures and the DSC performance. For cells with electrolyte #2, the Raman spectrum presented in Figure 6 shows that even 1% water in organic electrolyte does change the adsorption structure of EY on TiO_2 surface. After adding a small amount of water in acetonitrile, the 1618 cm^{-1} Raman peak tend to disappear while other peaks remain intact (the band at 1460 cm^{-1} is interfered with acetonitrile vibration features). This implies that the concentration of EY adsorption structure HM decreases with the presence of 1% water.

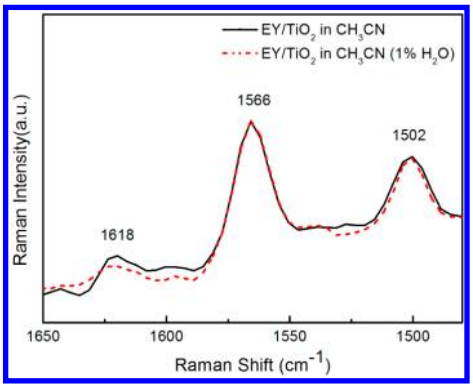

Figure 6. Raman spectrum for EY adsorbed TiO_2 in acetonitrile (black line) and acetonitrile containing 1% water (red).

Why do different adsorption configurations at the interface result in a marked change in the measured DSC photovoltaic performance, especially the persistent increase in V_{oc}? To answer this question, we perform first-principles calculations to illustrate the electronic structure of EY/TiO_2 of different interface configurations. The PBE exchange-correlation functional is employed in our calculation. It is well-known that GGA underestimates the absolute value of the TiO_2 band gap. However, the trend in band gap and the position of conduction band is reasonable. For instance, the calculated band gap difference between anatase and rutile TiO_2 is 0.24 eV, agreeing well with the experimental value of 0.21 eV.[29] Absolute position of CBE with respect to vacuum in EY/TiO_2 ranges from −4.32 to −4.16 eV (Figure 3), very similar to the experimental value (−4.4 eV).[30] The band gap of TiO_2 and organic molecules can be properly corrected if hybrid functionals are employed. They give similar results for the band alignment between the lowest unoccupied molecular orbital (LUMO) of the dye and TiO_2 CBE.

From the calculated projected density of states plots in Figure 5, the conduction band edge for the HM adsorption configuration (−4.32 eV) is lower than that for BB configuration (−4.26 eV) by about 60 meV. This trend matches well with the V_{oc} trend in DSC performance. Note that the measured V_{oc} corresponds to the energy difference between the quasi-Fermi level of TiO_2 under illumination (close to CBE) and the redox potential of the electrolyte.[1] The position of CBE is directly related to surface potential, affected by the dipole moments induced by dye adsorption. The calculated dipole moment of the BB mode is 1.02 D, larger than the HM mode (−0.89 D). According to the fact that the higher dipole moment shifts CBE to be more negative in potential,[31] an enhanced V_{oc} of BB adsorption mode can be inferred.

Transition from HM mode to BB mode also influences J_{sc} of DSC device by adjusting energy level position. First, the driving force for electron injection, namely, the energy difference between the CBE and the LUMO, is 1.0 eV for bidentate bridging adsorption. It is 0.1 eV higher than that for H-boned monodentate configuration (Figure 3), an important factor contributing to higher electron injection efficiency. According to Marcus theory (eq 1), electron transfer rate k_{ET} between two states is related to energy difference ΔG^0 between them (−0.9 eV for HM mode and −1.0 eV for BB mode in this case):

$$k_{ET} = \sqrt{\frac{\pi}{\hbar^2 \lambda k_B T}}\,|V|^2 \exp\left(\frac{-(\Delta G^0 + \lambda)^2}{4\lambda k_B T}\right) \quad (1)$$

Here λ is defined as reorganization energy and its value is taken as 1.0 eV, which is commonly accepted in previous works investigating similar dye/TiO_2 systems.[32,33] Since ΔG^0 for the BB mode is an optimized value (eq 1), it has a ~10% faster injection rate than HM mode at room temperature.

Second, the recombination, causing loss of J_{sc}, can be slowed down by adjusting the relative position of highest occupied molecular orbital (HOMO) and CBE. In our case, the energy difference varies between two states of structure. HM is −0.83 eV and BB is −0.76 eV (Figure 3). The λ value is 1.0 eV. Judging from eq 1, recombination rate in BB mode is about 30% slower than HM at 300 K. As a result, the HM adsorption structure is inferior to the BB structure in DSC applications when EY is used as the sensitizer, and one would minimize the presence of the former configuration to obtain better energy conversion characteristics.

The above discussion suggests that the addition of 1% water into the organic electrolyte results in 20−30% increase in DSC energy efficiency by suppressing unfavorable dye adsorption configurations on TiO_2. However, too much water is seldom applied in electrolytes and most experiments show that pure water electrolyte is harmful to DSC performance.[34,35] Our measurements on pure water based DSC (cell #4, Table 1) has reached only a low efficiency η = 0.2%, which is consistent with previous observations. Water induced efficiency losses have been attributed to formation of iodates,[36] electron lifetime decreases[37] and diffusion limitation of electron current.[38] A good balance must be retained between water-induced advantages such as adsorption structure selection and water-induced damages mentioned above. In this aspect, new

dx.doi.org/10.1021/jp404439p | J. Phys. Chem. C 2013, 117, 14659−14666

progresses are made very rapidly. In 2010, Law et al. fabricated pure water based DSCs achieving a high efficiency of 2.4%,[38] using Ru dye TG6 as a sensitizer. The value increased to 5.7% when water fraction is optimized to be 20% in methoxypropionitrile electrolyte. The trend is in nice agreement with our experiment; in the present work for EY-based DSCs, a good balance is reached by adding only a small amount of water, 1%, in acetonitrile solutions. A unique merit in the present work is that the improved photovoltaic performances in DSC devices are directly linked to the microscopic dye adsorption structures and electronic features at the dye/TiO_2 interface.

CONCLUSION

We present a detailed spectroscopic and computational study on improving photovoltaic performance by manipulating dye adsorption configurations on nanocrystalline TiO_2. EY adsorbed on TiO_2 can take either hydrogen-bonded monodentate configuration or bidentate bridging configuration in air and in solutions. Adding a small amount of water in organic electrolyte changes the pK_a value of the carboxyl group of EY and promotes deprotonation of the carboxyl, leading to a structural transition from the HM to BB adsorption. Consequently, the HM adsorption configuration, sensitive to the acidic environment and unfavorable in DSC applications, is suppressed by adding 1% water into acetonitrile electrolyte. We expect that this simple while effective method could be applied to other systems including devices with Ru complex and all-organic dyes, which also bind to TiO_2 via their carboxyl groups, to improve energy conversion efficiency of DSC devices. Efforts with more complex all-organic donor-π-acceptor dyes are under way. In addition, the present procedures on determining the microscopic interface structure for dye adsorption and establishing a direct link between interface structures and photovoltaic performance also provide new insights toward a complete understanding of DSC working mechanisms at the microscopic scale.

AUTHOR INFORMATION

Corresponding Author

*Tel: + 86-10-82649396. E-mail:smeng@iphy.ac.cn.

Notes

The authors declare no competing financial interest.

ACKNOWLEDGMENTS

We are grateful to Shifu Weng of Peking University for assistance in FTIR and Raman spectroscopy measurement. We also thank Shize Yang at Institute of Physics, Chinese Academy of Sciences for help in measuring photoabsorption spectra. The work is supported by NSFC (Grants 11074287 and 11222431), MOST (2012CB921403), and hundred-talent program of CAS.

REFERENCES

(1) O'Regan, B.; Grätzel, M. A Low-Cost, High-Efficiency Solar Cell Based on Dye-Sensitized Colloidal TiO2 Films. *Nature* **1991**, *353*, 737−740.

(2) De Angelis, F.; Fantacci, S.; Selloni, A.; Grätzel, M.; Nazeeruddin, M. K. Influence of the Sensitizer Adsorption Mode on the Open-Circuit Potential of Dye-Sensitized Solar Cells. *Nano Lett.* **2007**, *7*, 3189−3195.

(3) Jiao, Y.; Zhang, F.; Grätzel, M.; Meng, S. Structure−Property Relations in All-Organic Dye-Sensitized Solar Cells. *Adv. Funct. Mater.* **2013**, *23*, 424−429.

(4) Shklover, V.; Ovchinnikov, Y. E.; Braginsky, L. S.; Zakeeruddin, S. M.; Grätzel, M. Structure of Organic/Inorganic Interface in Assembled Materials Comprising Molecular Components. Crystal Structure of the Sensitizer Bis[(4,4′-carboxy-2,2′-bipyridine)(thiocyanato)]ruthenium-(II). *Chem. Mater.* **1998**, *10*, 2533−2541.

(5) Deacon, G. B.; Phillips, R. J. Relationships between the Carbon-Oxygen Stretching Frequencies of Carboxylato Complexes and the Type of Carboxylate Coordination. *Coord. Chem. Rev.* **1980**, *33*, 227−250.

(6) Nazeeruddin, M. K.; Humphry-Baker, R.; Liska, P.; Grätzel, M. Investigation of Sensitizer Adsorption and the Influence of Protons on Current and Voltage of a Dye-Sensitized Nanocrystalline TiO2 Solar Cell. *J. Phys. Chem. B* **2003**, *107*, 8981−8987.

(7) Lee, K. E.; Gomez, M. A.; Elouatik, S.; Demopoulos, G. P. Further Understanding of the Adsorption Mechanism of N719 Sensitizer on Anatase TiO2 Films for DSSC Applications Using Vibrational Spectroscopy and Confocal Raman Imaging. *Langmuir* **2010**, *26*, 9575−9583.

(8) Mali, S. S.; Betty, C. A.; Bhosale, P. N.; Patil, P. S. Eosin-Y and N3-Dye Sensitized Solar Cells (DSSCs) Based on Novel Nanocoral TiO2: A Comparative Study. *Electrochim. Acta* **2012**, *59*, 113−120.

(9) Sayama, K.; Sugino, M.; Sugihara, H.; Abe, Y.; Arakawa, H. Photosensitization of Porous TiO2 Semiconductor Electrode with Xanthene Dyes. *Chem. Lett.* **1998**, 753−754.

(10) Yu, Z.; Vlachopoulos, N.; Gorlov, M.; Kloo, L. Liquid Electrolytes for Dye-Sensitized Solar Cells. *Dalton Trans.* **2011**, *40*, 10289−10303.

(11) Jennings, J. R.; Liu, Y.; Wang, Q. Efficiency Limitations in Dye-Sensitized Solar Cells Caused by Inefficient Sensitizer Regeneration. *J. Phys. Chem. C* **2011**, *115*, 15109−15120.

(12) Kohn, W.; Sham, L. J. Self-Consistent Equations Including Exchange and Correlation Effects. *Phys. Rev.* **1965**, *140*, A1133−A1138.

(13) Perdew, J. P.; Chevary, J. A.; Vosko, S. H.; Jackson, K. A.; Pederson, M. R.; Singh, D. J.; Fiolhais, C. Atoms, Molecules, Solids, and Surfaces: Applications of the Generalized Gradient Approximation for Exchange and Correlation. *Phys. Rev. B* **1992**, *46*, 6671−6687.

(14) Kresse, G.; Hafner, J. Ab Initio Molecular Dynamics for Liquid Metals. *Phys. Rev. B* **1993**, *47*, 558−561.

(15) Lazzeri, M.; Vittadini, A.; Selloni, A. Erratum: Structure and Energetics of Stoichiometric TiO2 Anatase Surfaces [*Phys. Rev. B* 63, 155409 (2001)]. *Phys. Rev. B* **2002**, *65*, 119901.

(16) Cossi, M.; Rega, N.; Scalmani, G.; Barone, V. Energies, Structures, and Electronic Properties of Molecules in Solution with the C-PCM Solvation Model. *J. Comput. Chem.* **2003**, *24*, 669−681.

(17) McHedlov-Petrossyan, N. O.; Kukhtik, V. I.; Bezugliy, V. D. Dissociation, Tautomerism and Electroreduction of Xanthene and Sulfonephthalein Dyes in N,N-dimethylformamide and Other Solvents. *J. Org. Chem.* **2003**, *16*, 380−397.

(18) Seybold, P. G.; Gouterman, M.; Callis, J. Calorimetric, Photometric and Lifetime Determinations of Flourescence Yields of Fluorescein Dyes. *Photochem. Photobiol.* **1969**, *9*, 229−242.

(19) Moser, J.; Grätzel, M. Photosensitized Electron Injection in Colloidal Semiconductors. *J. Am. Chem. Soc.* **1984**, *106*, 6557−6564.

(20) Suttiponparnit, K.; Jiang, J.; Sahu, M.; Suvachittanont, S.; Charinpanitkul, T.; Biswas, P. Role of Surface Area, Primary Particle Size, and Crystal Phase on Titanium Dioxide Nanoparticle Dispersion Properties. *Nanoscale. Res. Lett.* **2011**, *6*, 27−34.

(21) Connor, P. A.; Dobson, K. D.; McQuillan, A. J. Infrared Spectroscopy of the TiO2/Aqueous Solution Interface. *Langmuir* **1999**, *15*, 2402−2408.

(22) Markuszewski, R.; Diehl, H. The Infrared Spectra and Structures of the Three Solid Forms of Fluorescein and Related Compounds. *Talanta* **1980**, *27*, 937−946.

(23) Wang, L.; Roitberg, A.; Meuse, C.; Gaigalas, A. K. Raman and FTIR Spectroscopies of Fluorescein in Solutions. *Spectrochim. Acta, Part A* **2001**, *57*, 1781−1791.

(24) Narayanan, V. A.; Stokes, D. L.; Vo-Dinh, T. Vibrational Spectral Analysis of Eosin Y and Erythrosin B—Intensity Studies for

Quantitative Detection of the Dyes. *J. Raman Spectrosc.* **1994**, *25*, 415−422.
(25) Lana-Villarreal, T.; Pérez, J. M.; Gómez, R. Adsorption Studies on Titanium Dioxide by Means of Raman Spectroscopy. *C. R. Chim.* **2006**, *9*, 806−816.
(26) Pászti, Z.; Guczi, L. Amino Acid Adsorption on Hydrophilic TiO2: A Sum Frequency Generation Vibrational Spectroscopy Study. *Vib. Spectrosc.* **2009**, *50*, 48−56.
(27) Nishikiori, H.; Uesugi, Y.; Takami, S.; Setiawan, R. A.; Fujii, T.; Qian, W.; El-Sayed, M. A. Influence of Steam Treatment on Dye−Titania Complex Formation and Photoelectric Conversion Property of Dye-Doped Titania Gel. *J. Phys. Chem. C* **2011**, *115*, 2880−2887.
(28) Pan, L.; Zou, J. J.; Zhang, X. W.; Wang, L. Water-Mediated Promotion of Dye Sensitization of TiO2 under Visible Light. *J. Am. Chem. Soc.* **2011**, *133*, 10000−10002.
(29) Reyes-Coronado, D.; Rodríguez-Gattorno, G.; Espinosa-Pesqueira, M. E.; Cab, C.; Coss, R. d.; Oskam, G. Phase-Pure TiO2 Nanoparticles: Anatase, Brookite and Rutile. *Nanotechnology* **2008**, *19*, 145605.
(30) Hagfeldt, A.; Grätzel, M. Light-Induced Redox Reactions in Nanocrystalline Systems. *Chem. Rev.* **1995**, *95*, 49−68.
(31) Pandey, S. S.; Lee, K. Y.; Hayat, A.; Ogomi, Y.; Hayase, S. Investigating the Role of Dye Dipole on Open Circuit Voltage in Solid-State Dye-Sensitized Solar Cells. *Jpn. J. Appl. Phys.* **2011**, *50*, 06GF08.
(32) Wiberg, J.; Marinado, T.; Hagberg, D. P.; Sun, L.; Hagfeldt, A.; Albinsson, B. Distance and Driving Force Dependencies of Electron Injection and Recombination Dynamics in Organic Dye-Sensitized Solar Cells. *J. Phys. Chem. B* **2010**, *114*, 14358−14363.
(33) Marinado, T.; Hagberg, D. P.; Hedlund, M.; Edvinsson, T.; Johansson, E. M. J.; Boschloo, G.; Rensmo, H.; Brinck, T.; Sun, L.; Hagfeldt, A. Rhodanine Dyes for Dye-Sensitized Solar Cells: Spectroscopy, Energy Levels and Photovoltaic Performance. *Phys. Chem. Chem. Phys.* **2009**, *11*, 133−141.
(34) Murakami, T. N.; Saito, H.; Uegusa, S.; Kawashima, N.; Miyasaka, T. Water-Based Dye-Sensitized Solar Cells: Interfacial Activation of TiO_2 Mesopores in contact with Aqueous Electrolyte for Efficiency Development. *Chem. Lett.* **2003**, *32*, 1154−1155.
(35) Saito, H.; Uegusa, S.; Murakami, T. N.; Kawashima, N.; Miyasaka, T. Fabrication and Efficiency Enhancement of Water-Based Dye-Sensitized Solar Cells by Interfacial Activation of TiO_2 Mesopores. *Electrochemistry* **2004**, *72*, 310−316.
(36) Macht, B.; Turrión, M.; Barkschat, A.; Salvador, P.; Ellmer, K.; Tributsch, H. Patterns of Efficiency and Degradation in Dye Sensitization Solar Cells Measured with Imaging Techniques. *Sol. Energy Mater. Sol. Cells* **2002**, *73*, 163−173.
(37) Jung, Y.-S.; Yoo, B.; Lim, M. K.; Lee, S. Y.; Kim, K. J. Effect of Triton X-100 in Water-Added Electrolytes on the Performance of Dye-Sensitized Solar Cells. *Electrochimi. Acta* **2009**, *54*, 6286−6291.
(38) Law, C. H.; Pathirana, S. C.; Li, X. O.; Anderson, A. Y.; Barnes, P. R. F.; Listorti, A.; Ghaddar, T. H.; O'Regan, B. C. Water-Based Electrolytes for Dye-Sensitized Solar Cells. *Adv. Mater.* **2010**, *22*, 4505−4509.